Project**: SEAWave**

Exposure dosimetry in animal and human studies

Work Package: WP5

Deliverable: D5.2

Deliverable No.: D16

Abstract

This deliverable provides a dosimetric characterization of millimeter-wave exposure in the animal and human health risk assessment studies of the SEAWave project, focusing on skin as the primary site of energy absorption. Age-dependent variability in murine skin properties was modeled and validated against power reflection measurements, enabling robust estimation of absorbed power density during early development. For the clinical study, individualized three-dimensional human skin models derived from optical coherence tomography (OCT) and ultrasound (US) imaging were implemented and experimentally validated, with automated segmentation enhancing efficiency. The results support reliable exposure assessment, correlation with potential biological outcomes, and cautious extrapolation between animal and human studies.

Project Details

Project name	SEAWave
Grant number	101057622
Start Date	01 Jun 2022
Duration	42 months
Scientific coordinator	Prof. T. Samaras, Aristotle University of Thessaloniki (AUTH)

Deliverable Details

Deliverable related number	D5.2
Deliverable No.	D16
Deliverable name	Report on dosimetry of exposure in animal and human studies
Work Package number	WP5
Work Package name	Macro and Microdosimetry in the Human and Murine Skin
Editors	Iakovidis S, Samaras T
Distribution	Public
Version	1.0
Draft/final	Draft
Keywords	Dosimetry, animal study, skin exposure, mmWave, human study, SEAWave-clin

Contents

1 Introduction 4
2 Objective 4
3 Materials and Methods 4
3.1 Model building framework 5
3.2 Skin models 7
3.3 Electromagnetic simulation ..... **Error! Bookmark not defined.**
4 Results and Discussion ..... **Error! Bookmark not defined.**
5 Conclusions 15
6 References ..... **Error! Bookmark not defined.**

1 Introduction

The deployment of millimeter-wave (MMW) technologies in emerging wireless communication systems has intensified the need for a detailed understanding of their interaction with biological tissues. Due to their short wavelengths, MMW fields exhibit shallow penetration depths, resulting in the skin being the primary site of energy absorption in both humans and experimental animals. Consequently, accurate dosimetric characterization of skin exposure is essential for interpreting biological effects, ensuring experimental reproducibility, and supporting reliable risk assessment.

Within this context, the current deliverable provides a comprehensive dosimetric assessment of MMW exposure in both murine and human models used in the health risk assessment studies of the SEAWave project. For the animal study, variability in skin morphology and dielectric properties during early postnatal development is explicitly considered to capture age-dependent differences in energy deposition. For the clinical study (SEAWave-Clin), an individualized modelling approach based on realistic three-dimensional skin reconstructions is employed and experimentally validated. Together, these investigations aim to quantify Absorbed Power Density (APD) in the skin, support the interpretation of potential biological outcomes in WP6 and WP7, and facilitate cautious extrapolation between animal and human exposure scenarios.

It should be noted that the dosimetry for the SEAWave-Clin study (i.e., the human study) is based on the data provided for the subjects recruited and irradiated until the end of the project.

2 Objective

The objective of the present deliverable is to provide a dosimetric characterization of the exposure to MMW radiation of animals and humans participating in the corresponding SEAWave studies. For the animal study (mice), dosimetric evaluations capturing variability in skin properties—namely layer thicknesses, dielectric properties, and hair content—are included for dorsal skin. For the clinical study an individualized approach was followed: the exposed skin areas of each participant (for both sham and real exposure) were three-dimensionally modeled and subsequently simulated using the framework presented in D5.3. These dosimetric evaluations add value to the results of WP6 (animal study) and WP7 (SEAWave-Clin study) by quantifying the electromagnetic power deposition within the skin and enabling correlation with the biological findings of these studies. They also support the extrapolation of findings from animals to humans, but only to the extent of different energy deposition patterns animal skin versus human skin when the same cell types or skin layers are considered.

3 Materials and Methods

The materials used and methods applied for the dosimetry characterization of the animal and human study (SEAWave-Clin) are presented in the following sections, §3.1 and §3.2 respectively.

3.1 Animal study

The materials and methods used for the dosimetry evaluation in the animal study were largely described in D5.1. A more detailed description can also be found in the corresponding publication in the *IEEE Journal of Microwaves* [1]. Therefore, they are not presented here for the sake of brevity.

In addition to the above, the validity of the developed model was assessed by comparing it with power reflection measurements (Figure 1).

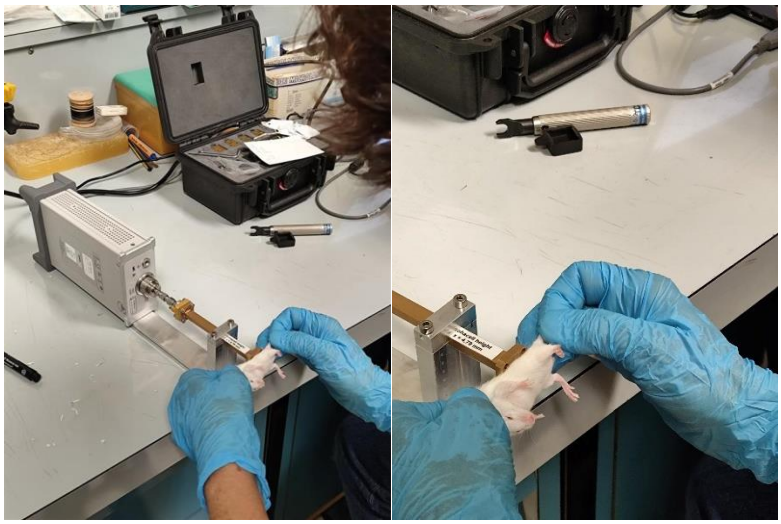

Figure 1: Photographs of the measurement setup used for power reflection measurements on living mice for model validation.

The measurement setup consisted of a WR28 open-ended rectangular waveguide with flanges from Eravant (Torrence CA, USA), connected to an Anritsu (Atsugi, Kanagawa, Japan) model MS46131A vector network analyzer (VNA). The frequency range of the measurements was 21–42 GHz. Mice from three different age groups were measured: postnatal day 5 (P5), 15 (P15) and 19 (P19). Each age group consisted of 6-8 animals of both sexes, and three sample measurements were taken for each mouse.

As reported in D5.1 and [1], measurements of skin-layer thicknesses were obtained from sacrificed mice at P2, P5, P15, and P21. These data were used as input parameters for the dosimetry model to enable direct comparison with measurements at P5 and P15. For P19, the corresponding skin-layer thickness values were estimated by linear interpolation of the median values between P15 and P21.

Significant deviations between the measurements and the model-predicted values of the power reflection coefficient were identified for P5 and P15, while a comparatively good agreement was observed for P19 (Figure 2). These deviations were attributed to the large uncertainty in the dielectric property values, resulting from both the limited availability and the large dispersion of Total Body Water (TBW) data reported in the literature (D5.1, Figure 4; [2]). In addition, different

mouse strains were used for measurements and modelling (inbred and outbred, respectively), further contributing to the variability. Therefore, a fitting procedure was applied to adjust the considered TBW values so that the model-predicted results aligned with the measurements. The fitting yielded higher TBW values than those predicted in D5.1, Figure 4 for P5 and P15 (85.1% and 77.7%, respectively), and an identical value for P19, as expected.

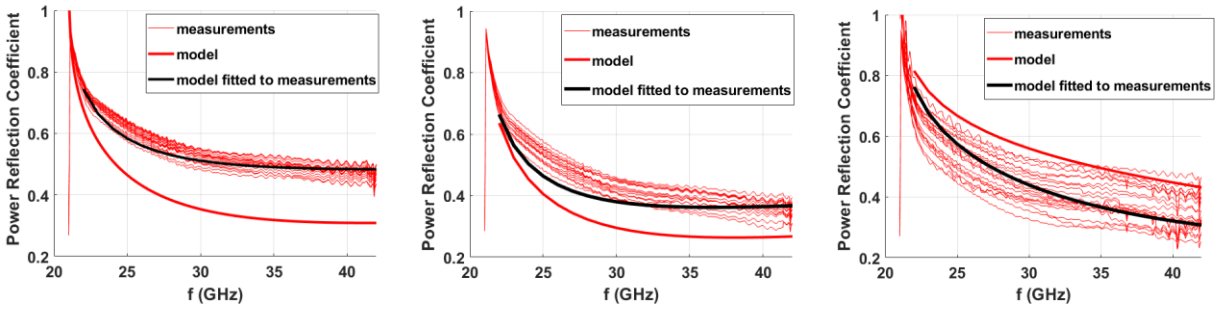

Figure 2: Measurements and model-predicted values for power reflection coefficient at different postnatal days: P5 (left), P15 (centre) and P19 (right).

The impact of the fitted TBW values—those aligned with the measurements—on dosimetry (i.e., APD) during the first hair cycle (P2–P21) was subsequently assessed. Figure 3 compares the original model-predicted APD values with those obtained from the fitted model. The fitted model yields APD values that fall within the full range of APD values predicted by the original model throughout the first hair cycle. In this context, the APD variability for murine skin predicted by the original model is considered adequate.

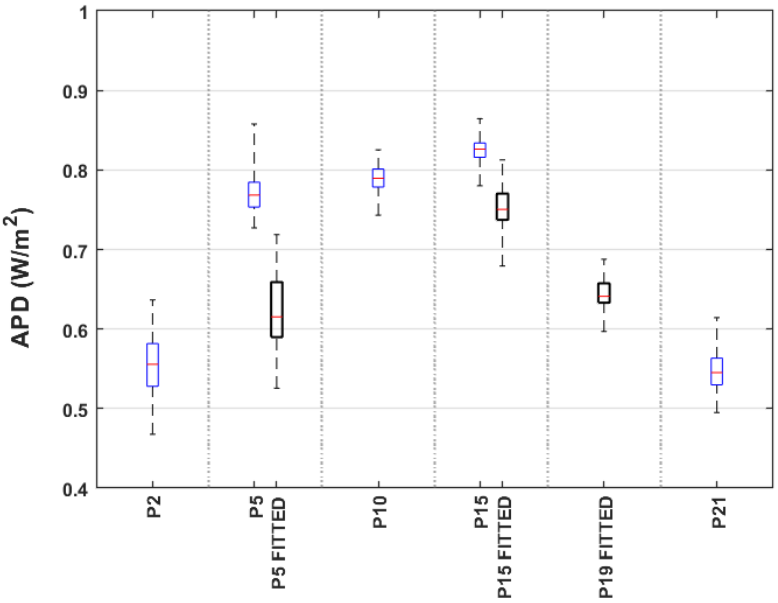

Figure 3: Comparison of predicted values for APD using the original model (blue boxplots) and the fitted model (black boxplots).

3.2 Human study

The dosimetry evaluation of the human study (SEAWave-Clin) followed an individualized approach: a separate model was developed for each participant. To this end, each participant had the exposed skin regions (including sham region) scanned using both Optical Coherence Tomography (OCT) and Ultrasound (US) imaging. The dimensional data acquired from these scans were then used to build realistic 3D skin models for the left and right inner arm of each participant. The framework developed for constructing the models and performing the dosimetry analysis has been described in detail in D5.3 and is therefore not reiterated here.

However, an important step affecting execution time was added to the original framework: the automation of the segmentation procedure in optical coherence tomography (OCT) images (D5.3, §3.1, Figure 1). In the following paragraphs, a description of the deep learning approach employed for the automatic segmentation of the OCT scan images is included.

Initially, a dataset of 2,400 grayscale OCT images was collected and manually annotated to create the reference ground truth contours for the two anatomical interfaces: the air–stratum corneum boundary and the epidermis–dermis junction. Manual segmentation was performed directly on the images by drawing the two contour lines for each case. The annotated dataset was randomly partitioned into 70% training, 15% validation, and 15% testing subsets, ensuring that the anatomical variability of the initial dataset was represented across all splits. The training set was used to optimize the segmentation model parameters, the validation set supported hyperparameter tuning and early stopping, and the independent test set was reserved for final performance evaluation.

Automatic contour detection was conducted using a Residual Encoder–Decoder Convolutional Neural Network (CNN) designed for pixel-wise segmentation. The encoder progressively extracts multi-scale features, whereas the decoder reconstructs a full resolution 2D probability map in which each column represents the probability distribution of the corresponding contour location. Residual blocks and skip connections improve gradient flow and preserve spatial detail. The predicted contour is obtained by selecting, for each column, the pixel with the highest probability value.

The model achieved high segmentation accuracy, exceeding 99% pixel-wise accuracy for the air–stratum corneum boundary and approximately 98% for the epidermis–dermis interface on the held-out test set. Although the predictions closely matched the ground truth, a small number of localized discontinuities (“spikes”) were observed, typically in low-contrast or structurally complex regions.

To ensure smoothness and anatomical consistency, a local smoothing procedure was applied as post-processing. The CNN output produces a 2D probability map that is first evaluated using a Local Stability Analysis, which assesses the reliability of each column prediction based on four criteria:

(i) small vertical change relative to neighboring columns (≤ 4 px),

(ii) proximity to a rolling median estimate (≤ 3 px deviation),

(iii) sufficiently high peak probability (≥ 0.2), and

(iv) clear separation from the second-highest probability (≥ 0.05).

Columns meeting all criteria are considered stable and are locked, remaining unchanged. Columns that fail one or more criteria are treated as unstable and undergo optimization. Localized smoothing then refines only these regions using a Viterbi-based dynamic programming algorithm, which identifies the most probable continuous path across columns while preserving the original stable segments. This combined approach effectively eliminates spikes and yields smooth, anatomically consistent contours.

Another addition was made to the original framework (described in D5.3) in order to capture variations in dosimetry induced by changes in the dielectric properties of the skin layers. To this end, we followed the same approach as in the case of murine skin (D5.1), also described in [3], [4]: the use of Total Body Water (TBW) as a proxy for evaluating age-related variations in dielectric properties (Figure 4).

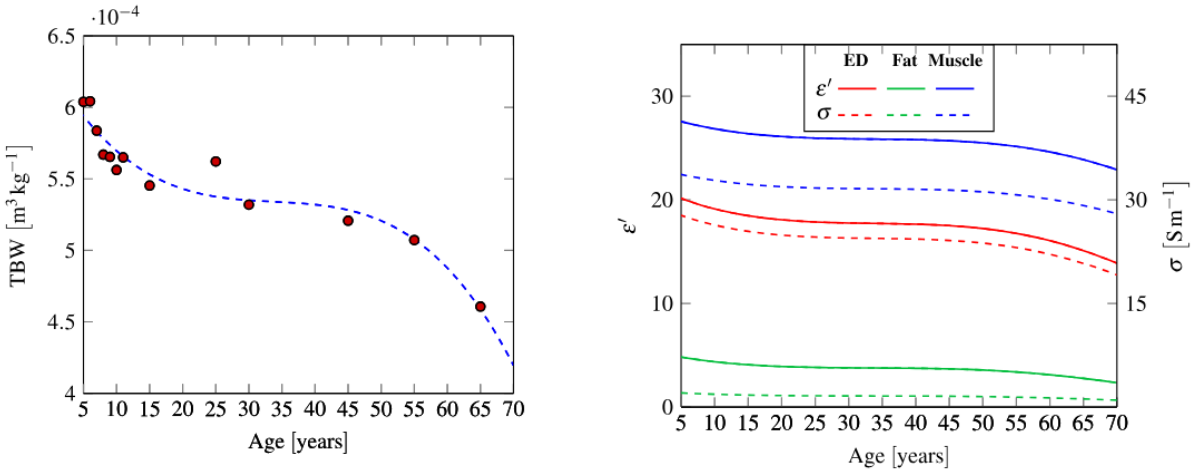

Figure 4: Total Body Water (TBW) as a function of age (left) and the corresponding variations in dielectric properties (right). Figures taken from *Sacco et al.* [3].

To validate the developed framework for human skin dosimetry assessment, power reflection measurements were performed. Three healthy volunteers (two females and one male) first underwent OCT and US skin scanning, followed by measurement sessions. The same skin region examined in SEAWave-Clin —the inner arm—was used for validation. Measurements of the power reflection coefficient were conducted using the same setup as in the mouse experiments (Figure 1). The dimensional data from OCT and US were subsequently used to build 3D skin models for each volunteer, which were then simulated in Sim4Life following the established framework (Figure 5).

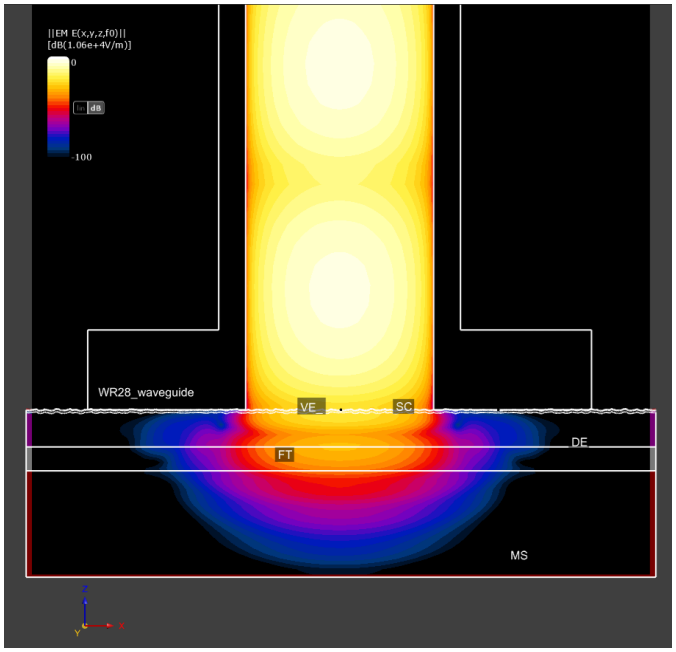

Figure 5: Colormap of E-field values on a cross-sectional plane of the waveguide-3D skin simulated model at 27.5 GHz used for comparison with the measurement data.

Simulations were performed at discrete frequencies (22.5, 25, 27.5, 30, 32.5, 35, 37.5, 40 and 42 GHz) within the measurement frequency range (21-42 GHz). Figure 6 presents the comparison between measurement data and model-predicted values for the power reflection coefficient. A good agreement is observed, with deviations remaining below 14.6% (i.e., 0.6 dB).

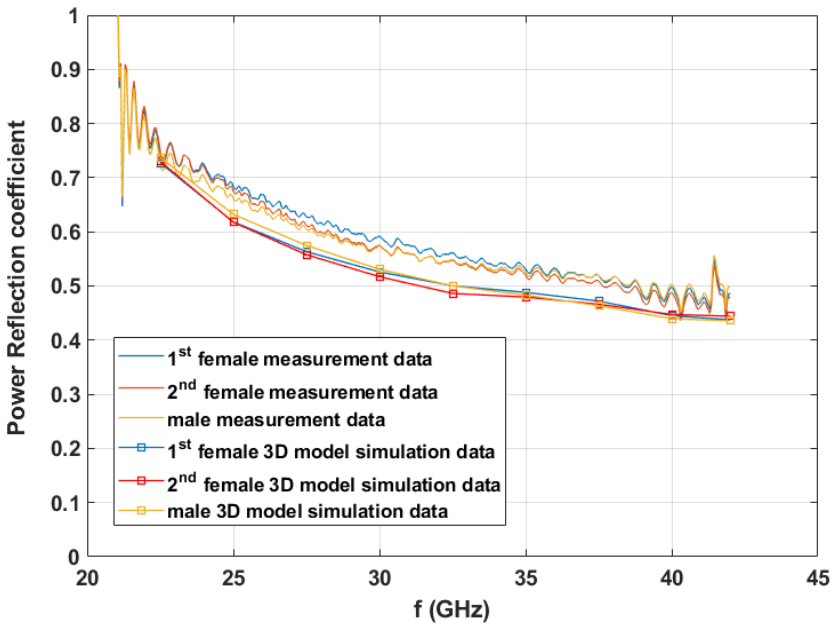

Figure 6: Power reflection coefficient as evaluated from VNA measurements (continuous lines) and from simulation data using 3D realistic skin models and a WR28 waveguide model (continuous lines with squared markers).

4 Results and Discussion

4.1 Animal study

The dosimetry for the animal study is reported in D5.1, and a more detailed presentation of the dosimetry results can also be found in [1]. The aforementioned sources provide results based on an incident power density of 1 W/m². However, these results can be straightforwardly extrapolated to the incident power densities applied in the animal study: 6.67 W/m² for the Low Power Density (LPD) chamber and 20 W/m² for the High Power Density (HPD) chamber.

Figure 7 shows the variation in the APD distribution throughout the first hair cycle for both the LPD and HPD chambers. Within the LPD chamber, the APD in murine skin varies within the [3.1, 5.8] W/m² range, whereas within the HPD chamber it varies within the [9.4, 17.3] W/m² range. It is worth noting that this variability reflects variations in both skin layer thickness and dielectric properties.

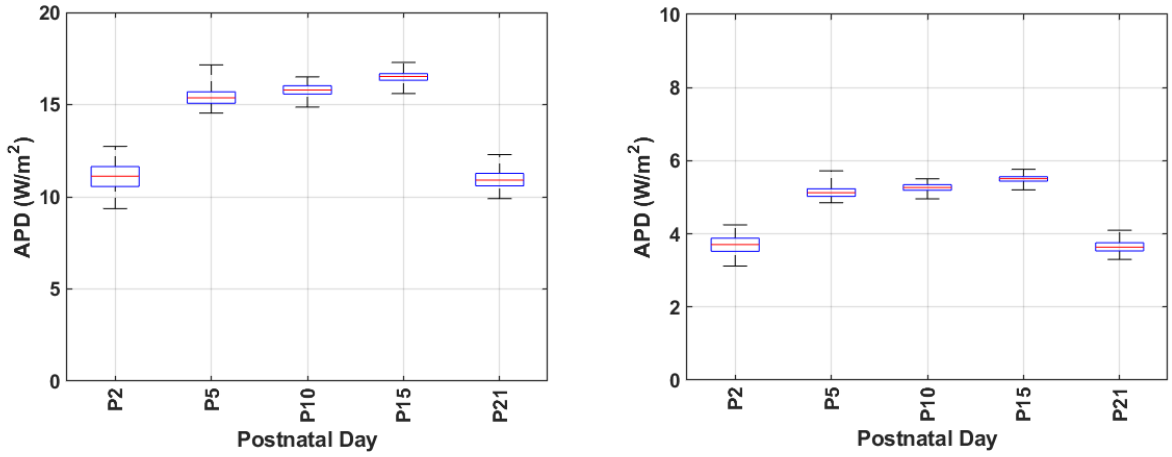

Figure 7: Absorbed Power Density (APD) in murine skin during the first hair cycle (P2-P21).

The homogeneity range of the field inside the chamber ([72%, 133%], in terms of incident power density) needs to be added to the aforementioned ranges (Table 1, Figure 8)

Table 1: Variation of incident power density at different cage positions as a percentage of the nominal value.

Position	Incident Power Density (% of nominal)
1	133
2	108.5
3	113.2
4	93.4
5	79.8
6	72

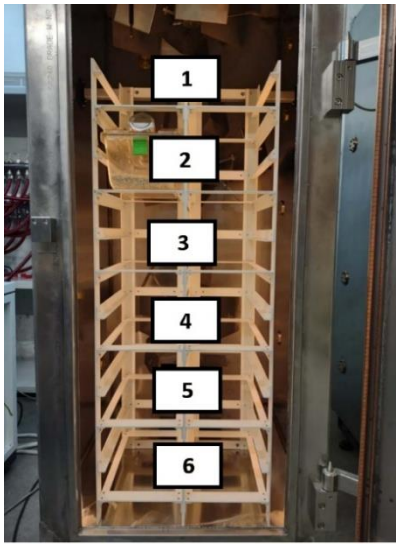

Figure 8: Cage position numbering inside the exposure chamber with respect to field homogeneity.

Cage positions are rotated within the chamber to ensure that all cages spend equal time at each of the six positions, thereby alleviating potential exposure differences among cages. It is worth noting that even with the field inhomogeneity included, the APD intervals do not overlap compared on a per postnatal day basis (Table 2).

Table 2: APD difference between maximum APD for LPD chamber and lower APD for HPD chamber, including chamber inhomogeneity.

Postnatal Day	APD difference (dB)
2	0.77
5	1.39
10	1.65
15	1.66
21	1.16

The initial “guard band” of 4.77 dB (i.e., 20·log(20/6.67)) between LPD and HPD for the nominal power density values (6.67 W/m² and 20 W/m², respectively) is substantially reduced, yet not exceeded, on any postnatal day (Table 2).

Finally, the focus on the first hair cycle (P2–P21) is justified by the fact that the largest variability in skin layer thickness and dielectric properties occurs during this period.

4.2 Human study

Table 3 summarizes the demographic characteristics of the SEAWave-Clin volunteers who, at the time of writing (end of the project), have participated in the study. Participants so far belong to three groups, i.e., healthy subjects, patients with atopic dermatitis and patients with genetic

diseases. No participants with dermatoporosis, i.e., those belonging to the fourth group of the clinical trial, have been exposed so far. It is worth noting that none of the participants, including those with pre-existing conditions, exhibited clinical signs of their condition in the exposed skin area. However, even in clinically unaffected skin of patients with atopic dermatitis, changes in epidermal water content (i.e., in the SC and VE layers) have been reported in the literature, [5], [6]. These changes lead to corresponding alterations in the dielectric properties of the SC and VE, which were evaluated using the previously mentioned approach based on Lichtenecker's logarithmic formula (D5.1).

Table 3: SEAWave-clin participants' descriptive information

Participant's No	Participant's ID	Sex	Age	Group
1	CJ	female	76	Genetic disease
2	MT	male	25	Healthy
3	VE	male	24	Healthy
4	CW	female	22	Healthy
5	GG	male	23	Healthy
6	FD	female	22	Healthy
7	AS	female	23	Healthy
8	ID	male	18	Healthy
9	YT	female	21	Healthy
10	AC	male	24	Healthy
11	GD	female	24	Healthy
12	LV	male	22	Healthy
13	CO	female	22	Healthy
14	GV	male	42	Atopic dermatitis
15	MS	female	65	Atopic dermatitis
16	PS	male	64	Atopic dermatitis
17	FC	male	56	Atopic dermatitis
18	AG	male	31	Atopic dermatitis
19	ET	female	26	Atopic dermatitis
20	CZ	female	38	Atopic dermatitis
21	LG	female	23	Healthy

Participant's No	Participant's ID	Sex	Age	Group
22	SM	female	23	Healthy
23	PB	male	18	Healthy
24	VJ	male	24	Healthy
25	MD	female	65	Genetic disease

Figure 9 presents the statistical distribution of individual skin layer thicknesses, as evaluated from the 50 3D skin models, using boxplot charts. Because the boundaries of the Stratum Corneum (SC) in thin-skin regions are difficult to discern in conventional OCT scan images, a constant thickness value (21.8 µm, [7]) was considered. Moreover, the muscle (MS) layer thickness is comparatively large at the exposed skin area (inner arm); a value of 4 mm was deemed sufficient for modelling, as larger values only increase the computational domain and associated resources without affecting the dosimetry. Finally, a matching layer (D7.2, Figure 2.4) was added on top of the skin models, with a thickness of 0.95mm and ε_r=6.4 and σ=0 S/m.

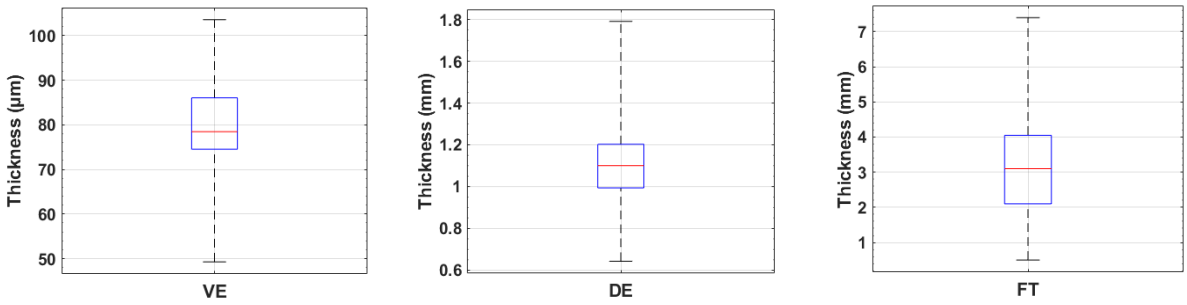

Figure 9: Boxplot distributions of individual skin layer thicknesses for both arms of the participants: Viable Epidermis (VE) on the left, Dermis (DE) in the center, and Fat (FT) on the right. The dashed line edges correspond to the minimum and maximum values of each distribution.

Table 4 presents the absorbed power density (APD) of the skin for each arm of each participant. The incident power density is 20 W/m². The use of a matching layer in the exposure setup results in an increase in APD for each participant and a reduction in APD variability across participants, compared with a hypothetical scenario without a matching layer (0.5dB versus 1.1dB), Figure 10.

Table 4: SEAWave-clin participants' Absorbed Power Density (APD) in W/m²

Participant's No	Participant's ID	APD (W/m²) Left arm	APD (W/m²) Right arm
1	CJ	17.61	17.67
2	MT	19.41	19.43
3	VE	19.10	19.10

Participant's No	Participant's ID	APD (W/m^2) Left arm	APD (W/m^2) Right arm
4	CW	19.49	19.54
5	GG	19.46	19.33
6	FD	19.66	19.75
7	AS	19.66	19.65
8	ID	19.60	19.58
9	YT	19.62	19.65
10	AC	19.60	19.69
11	GD	19.80	19.79
12	LV	19.21	19.23
13	CO	19.41	19.53
14	GV	19.09	19.46
15	MS	19.72	18.39
16	PS	18.91	18.71
17	FC	19.39	19.65
18	AG	19.13	19.11
19	ET	19.80	19.83
20	CZ	19.53	19.56
21	LG	19.47	19.43
22	SM	19.63	19.62
23	PB	19.35	19.72
24	VJ	19.83	19.12
25	MD	18.76	18.74

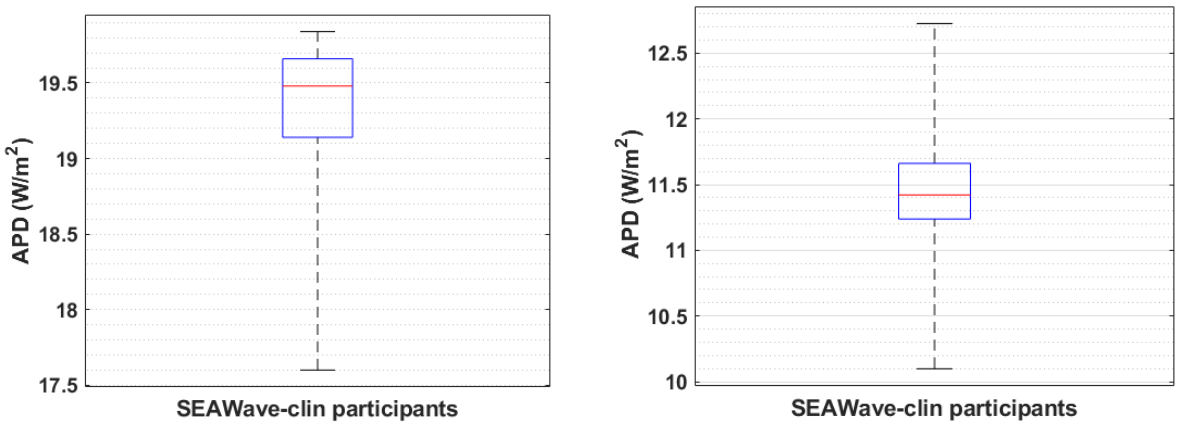

Figure 10: Boxplot distribution of Absorbed Power Density (APD) for 25 SEAWave-Clin participants (both arms) with a matching layer (left) and for the case without a matching layer (right).

Variations in APD across participants reflect both the differing dimensional characteristics of their skin models and the variation in dielectric properties of their skin layers induced by age-related changes in total body water (TBW), as well as variations in the water content of epidermis in atopic dermatitis group. However, the use of the matching layer limits APD variability, thereby increasing the homogeneity of exposure among participants. At the same time, the individualized modelling approach reduces uncertainty in the dosimetry evaluation for each participant, thus facilitating the correlation of potential biological findings with induced fields in the skin.

5 Conclusions

This deliverable provides a comprehensive dosimetric characterization of millimeter-wave exposure in both the animal and human components of the SEAWave project. For the animal study, the developed murine skin model successfully captured the substantial variability in absorbed power density arising from age-dependent changes in skin layer thickness, dielectric properties, and hair development during the first hair cycle. Although discrepancies between measured and simulated power reflection coefficients were initially observed, these were systematically addressed through a fitting procedure based on total body water. The resulting dosimetric estimates remained within the variability bounds of the original model, supporting its robustness and suitability for interpreting biological outcomes in WP6 and for informing cautious extrapolation between murine and human exposure scenarios.

For the SEAWave-clin study, an individualized dosimetry framework based on realistic 3D skin models was successfully implemented and validated against experimental power reflection measurements. The integration of automated OCT image segmentation using a deep learning approach substantially improved efficiency while preserving high anatomical accuracy. The results demonstrate that, despite inter-individual differences in skin morphology and age-related dielectric properties, the use of a matching layer effectively reduced variability in absorbed

power density and enhanced exposure homogeneity across participants. Overall, this individualized and validated dosimetric approach strengthens the reliability of exposure assessment in the clinical study and provides a solid basis for correlating observed biological responses with localized energy deposition in human skin.

6 References

[1] S. Iakovidis, S. Leonardi, E. Fratini, S. Pazzaglia, M. Mancuso, and T. Samaras, "Murine Skin Dosimetry Under Millimeter Wave Exposure," *IEEE Journal of Microwaves*, vol. 4, no. 2, pp. 204–212, Apr. 2024, doi: 10.1109/JMW.2023.3345133.

[2] C. B. Bailey, W. D. Kitts, and A. J. Wood, "Changes in the gross chemical composition of the mouse during growth in relation to the assessment of physiological age," *Can J Anim Sci*, vol. 40, no. 2, pp. 143–155, 1960, doi: 10.4141/cjas60-022.

[3] G. Sacco, S. Pisa, and M. Zhadobov, "Age-dependence of electromagnetic power and heat deposition in near-surface tissues in emerging 5G bands," *Sci Rep*, vol. 11, no. 1, Dec. 2021, doi: 10.1038/s41598-021-82458-z.

[4] J. Wang, O. Fujiwara, and S. Watanabe, "Approximation of aging effect on dielectric tissue properties for SAR assessment of mobile telephones," *IEEE Trans Electromagn Compat*, vol. 48, no. 2, pp. 408–413, May 2006, doi: 10.1109/TEMC.2006.874085.

[5] M. Egawa, T. Hirao, and M. Takahashi, "In vivo estimation of stratum corneum thickness from water concentration profiles obtained with raman spectroscopy," *Acta Derm Venereol*, vol. 87, no. 1, pp. 4–8, 2007, doi: 10.2340/00015555-0183.